Advanced Steel Construction – Vol. 21 No. 5 (2025) 448–457
DOI:10.18057/IJASC.2025.21.5.7

SEISMIC PERFORMANCE OF PU-PAI FANG-DOVETAIL TENON JOINTS WITH VARYING LOOSENING DEGREES REINFORCED BY STEEL SLEEVE CLAMP HOOPS

Sen-Long Tan [1], Yun-Peng Chu [1], Yao-Peng Liu [2,*], Jia-Hao Wang [1], Si-Qi Wang [1], Zheng Zhang [3] and Bo Si [4]

[1] *School of Civil Engineering and Architecture, Southwest University of Science and Technology, Mianyang 621010, China*
[2] *School of Civil Engineering and Transportation, South China University of Technology, Guangzhou 510641, China*
[3] *Tongji Architectural Design (Group) Co., Ltd, Shanghai 200092, China*
[4] *Beijing Building Construction Research Institute, Beijing 10039, China*
** (Corresponding author: E-mail: yaopengliu@scut.edu.cn)*

ABSTRACT

The Pu–pai Fang-dovetail tenon joint, an enhanced form of the traditional dovetail joint, is commonly used at beam-column connections in traditional beam-lifting timber structures. However, long-term environmental exposure and seismic loading often lead to wood shrinkage and joint loosening, reducing structural integrity. This study proposes a reinforcement method for Pu-pai Fang–dovetail tenon joints with varying degrees of looseness using steel sleeve clamp hoops. Quasi-static tests were conducted on one intact specimen and three specimens with different looseness levels to examine their failure modes and seismic behavior. Results indicate that tenon pull-out in the reinforced joints causes tearing of wood fibers at the mortise and Pu-pai Fang, yet the flexural capacity continues to increase without exhibiting a descending branch. The energy dissipation capacity and stiffness degrade rapidly at first and then stabilize. Compared with unreinforced joints, the reinforced specimens exhibited a lower tenon extraction rate and higher ultimate flexural capacity. A finite element model was subsequently developed, showing good agreement with the experimental results. Parametric analysis revealed that selecting an appropriate friction coefficient (0.3–0.5) and clamp-hoop thickness (5–7mm) can effectively improve the seismic performance of Pu-pai Fang–dovetail tenon joints.

ARTICLE HISTORY

Received: 15 June 2025
Revised: 28 July 2025
Accepted: 11 August 2025

KEYWORDS

Ancient timber buildings;
Pu-pai Fang-Dovetail tenon joints;
Loosening degrees;
Quasi-static test;
Parametric analysis

1. Introduction

The dovetail tenon joint is a commonly used key joint form for the connection between beams and columns in traditional beam-lifting timber structures [1]. Under the action of earthquakes, the tenon and mortise effectively prevent the tenon from being pulled out and falling off by mutual friction, sliding and compression deformation. This structural form belongs to a typical "semi-rigid" connection and has a good energy dissipation and shock absorption effect [2,3,4,5]. However, the cutting behavior at the end of the column to achieve the connection between the column and the beam frame layer significantly weakens the load-bearing capacity of the column and also provides the initial conditions for the invasion of microorganisms into the wood. Due to the long-term exposure of ancient timber structures to the natural environment and the characteristic of wood materials that they tend to shrink easily, cracks generally occur in the beam and column components under the long-term load and the influence of wind and rain, as shown in **Fig. 1**(a), and the connection points of the joints become loose, as shown in **Fig. 1**(b). These deterioration phenomena cause the seismic performance of timber structures to deteriorate, making them prone to premature damage during earthquakes. The failure of key joints may lead to the overturning and collapse of the entire structure.

In recent years, some scholars have carried out a large number of experimental studies on the mechanical properties and seismic resistance of traditional mortise and tenon joints caused by loose damage [6]. The bending moment, stiffness and energy dissipation capacity of the loose joints were all lower than those of the intact joints. Moreover, the greater the degree of looseness of the loose joints, the lower the bearing capacity, and the more obvious the degradation of stiffness and strength. However, they still had good deformation capacity. Zhang et al. [7] found through numerical analysis that the extrusion deformation of the joints was mainly concentrated at the tenon of the dovetail tenon, the equivalent plastic strain of the tenon increased linearly, the failure at the end of the tenon was the least, and the failure at the neck of the tenon was the greatest. Yu et al. [8] established the geometric deformation characteristics and geometric model of the dovetail tenon and found that the bending moment of the dovetail tenon connection is directly proportional to the height and length of the tenon. Considering the gap effect caused by loosening is of great significance for performance degradation and the establishment of bending moment models [9]. Bai et al. [10,11] explained how loosening damage affects the failure mode and mechanical properties of dovetail joints. He et al. [12] proposed a theoretical bending moment model for loose joints and verified it through the deformation characteristics and lateral resistance of the timber frame. At present, the research on loose joints mainly focuses on traditional mortise and tenon joints. The ingenious design of ancient architectural timber structures is to design Pu-pai Fang on the upper part of beam components to enhance the bending resistance of the structure. Such joints are called Pu-pai Fang - dovetail tenon joints [13]. At present, some scholars have conducted relatively few studies on the mechanical properties of Pu-pai Fang components [14,15]. The Pu-pai Fang can significantly enhance the rotational stiffness and bending moment of joints. The force mechanism of this type of joint is significantly different from that of other traditional joints, but it also faces problems such as the deterioration of structural performance state under environmental influence, as shown in **Fig. 1**(c). Therefore, conducting research on the Pu-pai Fang-Dovetail tenon joint with different degrees of looseness is of great significance for quantitatively assessing the damage state of the timber structures of ancient buildings.

The timber structures of ancient buildings have problems such as deformation, cracking, decay, tenon pull-out and damage by wood-boring insects during long-term use, which seriously affect the structural safety and protection and inheritance [16]. Meanwhile, the damage to timber structures often occurs at the joints, which in turn significantly affects the stability of the overall structure. Therefore, there is an urgent need to formulate effective protective measures for timber structures, especially for joints. The common reinforcement methods for joints in ancient buildings mainly include steel components [17,18,19], fiber cloth, dampers [20,21,22], et al. By comparing the above-mentioned reinforcement methods, it is found that the steel components assembled with flat steel, iron hooks and clips are complex and prone to cause significant damage to wood. However, CFRP reinforcement usually requires wrapping the entire mortise and tenon joint. Dampers are relatively expensive. These reinforcement methods are prone to causing damage to the cultural relics themselves and subsequent pollution, which is contrary to the principles of protection and restoration of cultural relic buildings, and the improvement in their mechanical properties is limited. He et al. [23] used wooden wedges to reinforce the straight tenons, which did not cause damage to the main body of the cultural relic building. The rotational stiffness and load-bearing capacity were significantly improved, but new deterioration risks may occur in the natural environment. Therefore, it is urgent to provide a reinforcement method that is convenient to implement, inexpensive, and does not cause deterioration to the main body of cultural relic buildings.

This paper presents a steel sleeve clamp hoop reinforcement device and conducts Quasi-static test tests on one intact specimen and three specimens with different loosening conditions. The working mechanism and seismic performance of reinforcing the Pu-pai Fang - dovetail tenon joint under different loosening degrees are systematically studied. In addition, a finite element model was established to conduct parametric analysis on the friction coefficient, bolt preload, and thickness of the Pu-pai Fang clamp hoop, and the influence of these factors on the seismic performance of the joints was discussed.

Fig. 1 Typical damage conditions of mortise-and-tenon joints in ancient timber structures

2. Joint characteristics and force mechanism

2.1. Joint characteristics

According to the records in the Song Dynasty's "Yingzao Fashi" [24], in the official-style buildings, the beam and column components were often connected by dovetail tenon joints. The column ends were successively stacked with Lu-Tou and Tou-Kung and other components upwards through Man-Tou tenon joint, forming an important anti-lateral system [25]. The structural features are shown in **Fig. 2**. The tenon has a structure that is wider on the outside and narrower on the inside, with the mortise being larger on the inside and smaller on the outside. The tenon is precisely embedded into the mortise of the column, forming an interlocking connection. The traditional dovetail tenon joint, as shown in **Fig. 3**(a), there is a Pu-pai Fang component designed above the dovetail tenon, as shown in **Fig. 3**(b). The upper part of the Pu-pai Fang components can be classified into dovetail tenon joints and Pu-pai Fang-dovetail tenon joints according to whether they are equipped with Pu-pai Fang-dovetail tenon joints.. The Pu-pai Fang-dovetail tenon joint suppresses rotational deformation through the enhanced stiffness provided by the common parapet beam, and the geometric constraints formed effectively prevent the tenon from being pulled out. The Pu-pai Fang-dovetail tenon joint is widely used in traditional timber structure buildings.

2.2. Force mechanism

For the standardized description, forward loading is defined as the clockwise rotation of the beam, reducing the Angle between the beam and the column to below 90 °, while reverse loading occurs during counterclockwise rotation, causing the Angle to exceed 90 °, as shown in **Fig. 4**. Under forward loading, as shown in **Fig. 4** (a), the beam is constrained and rubbed by the mortise during rotation, and the tenon is locally embedded and pressed, forming horizontal pressure and reverse resistance. The wood in the compressed area is crushed. The Pu-pai Fang rotates in the same direction as the beam. Due to the limiting effect of the mortise of the Man-Tou tenon joint, the Pu-pai Fang first generates reverse resistance and effectively restricts the rotation behavior of the beam. This behavior is not tying but eventually leads to the separation of the beam and the Pu-pai Fang. Under reverse loading, as shown in **Fig. 4**(b), during the rotation of the Pu-pai Fang, it first comes into contact with the column end and forms resistance and horizontal shear force. Meanwhile, the tenon forms an outward horizontal shear force on the mortise during the rotation process. This behavior also prevents the beam and the Pu-pai Fang from rotating synchronously, eventually resulting in the separation at the connection point. However, the further increase in the rotation of the joints causes the wood to enter the plastic deformation stage. During the mutual compression process between the tenon and the mortise, the tenon is gradually pulled out, resulting in cumulative plastic deformation of the tenon. Due to insufficient restraint capacity, the wood fibers at the mortise tear, as shown in **Fig. 4**(c). The Pu-pai Fang becomes the main load-bearing component during the process of restricting the structural rotation. The main occurrence of wood fiber tearing and end shear damage along the wood grain direction of the Pu-pai Fang.

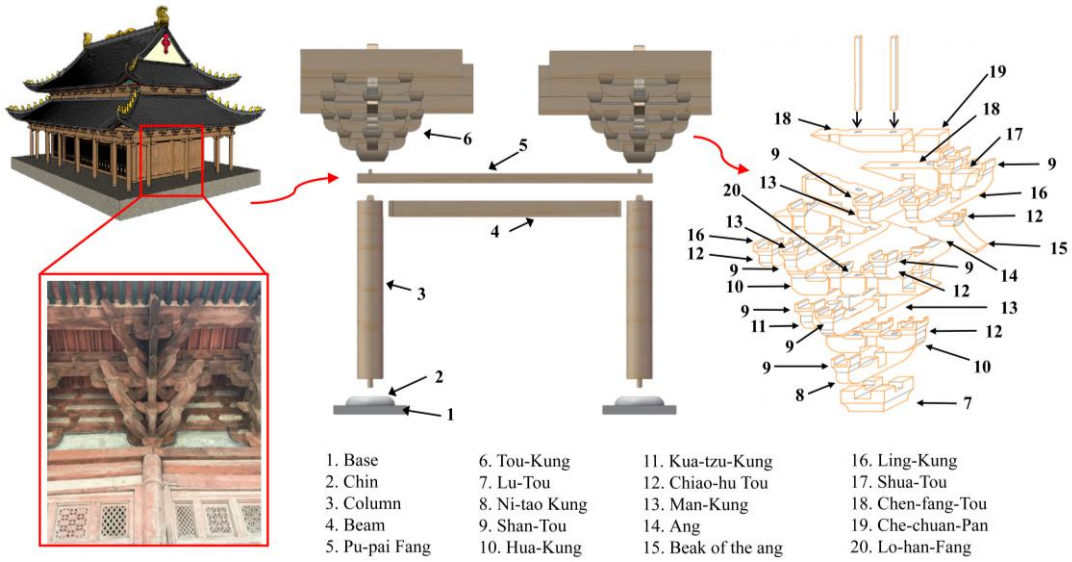

Fig. 2 Structural features of timber structures in ancient buildings

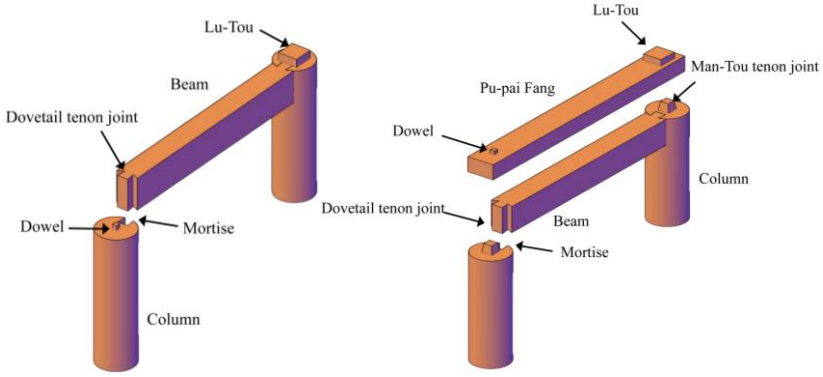

(a) Traditional dovetail tenon joint (b) Designed Pu-pai Fang above the dovetail tenon joint

Fig. 3 Construction characteristics of Pu-pai Fang-dovetail tenon joints

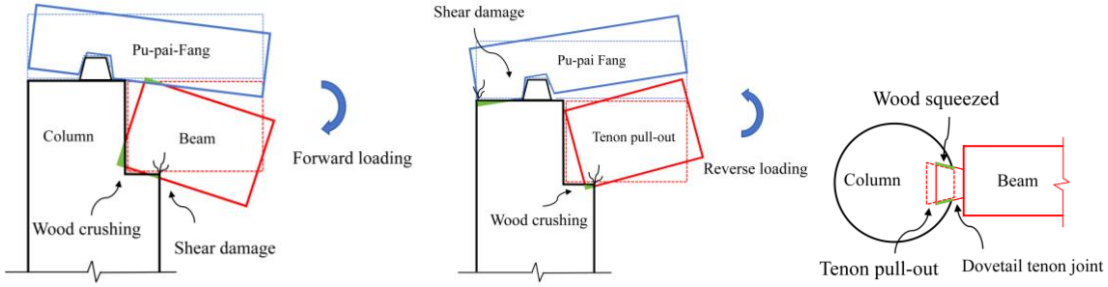

(a) Forward loading (b) Reverse loading (c) Joint interface

Fig. 4 Force mechanism of the Pu-pai Fang-dovetail tenon join

3. Quasi-static test

3.1. Specimen design

This test mainly focuses on the use of a steel sleeve clamp hoop reinforcement device that is simple, portable, low-cost and will not cause secondary damage to the cultural relics buildings themselves. The purpose of the test is to research the seismic performance of the steel sleeve clamp hoop reinforcement of Pu-pai Fang - dovetail tenon joints with different degrees of looseness. The design of the joint reinforcement is shown in **Fig. 5**. According to the secondary wood size standards stipulated in the Song Dynasty architectural classic "Yingzao Fashi", the specimens were made at a scale of 1:3.52. The specific dimensions are shown in **Fig. 6.** The side view and top view of the Pu-pai Fang-dovetail tenon joint are shown in **Fig. 6**(a) and **Fig. 6**(b), respectively. Due to the fact that bolts have strong ultimate resistance and ductility [26]. The joints are fixed by a reinforcing device composed of beam-column support component, Pu-pai Fang clamp hoops and column clamp hoop. The beam-column support component and column clamp hoop are connected by movable bolts. The Pu-pai Fang clamp hoops are formed by welding rectangular clamps with bolts [27,28]. The Pu-pai Fang clamp hoops and beam-column support component are connected by welded bolts. The specific dimensions are shown in **Fig. 7**, **Fig.8** and **Fig.9**. The side view, front view and top view of the beam-column support component are shown in **Fig. 7**(a), **Fig. 7**(b) and **Fig. 7**(c), Side view, front view and top view of Pu-pai Fang clamp hoop, as shown in **Fig. 8**(a), **Fig. 8**(b) and **Fig. 8**(c), Top view, front view and side view of column clamp hoop, as shown in **Fig. 9**(a), **Fig. 9**(b) and **Fig. 9**(c) Due to the differences in the degree of shrinkage and aging of wood, the Pu-pai Fang - dovetail tenon joints became loose to varying degrees. The specimens were made by reducing the length of the tenon to simulate different degrees of loosening, and one intact joint and three specimens with different loose joints were fabricated (**Table 1**).

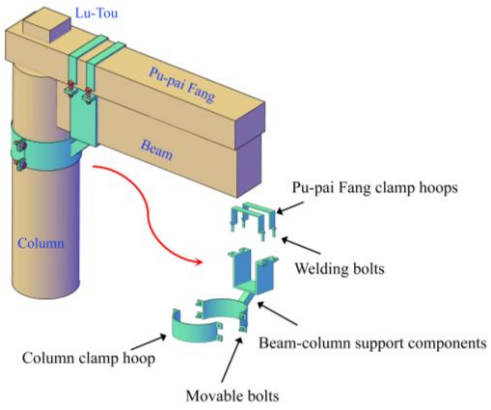

Fig. 5 Steel sleeve clamp hoops reinforce the Pu-pai Fang - dovetail tenon joint design

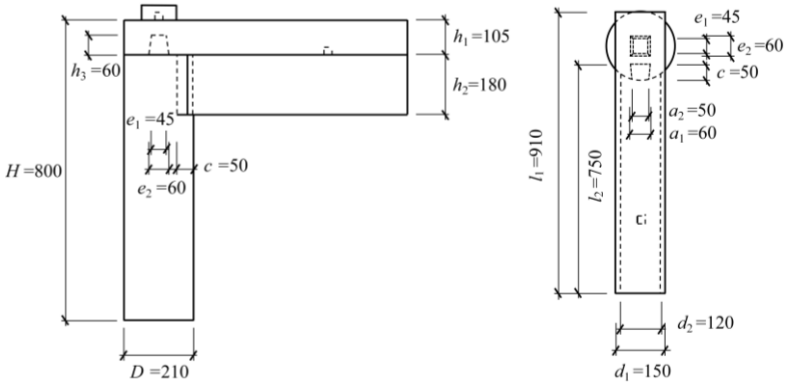

(a) Side view (b) Front view

Fig. 6 Detailed dimensions of Pu-pai Fang-dovetail tenon joint

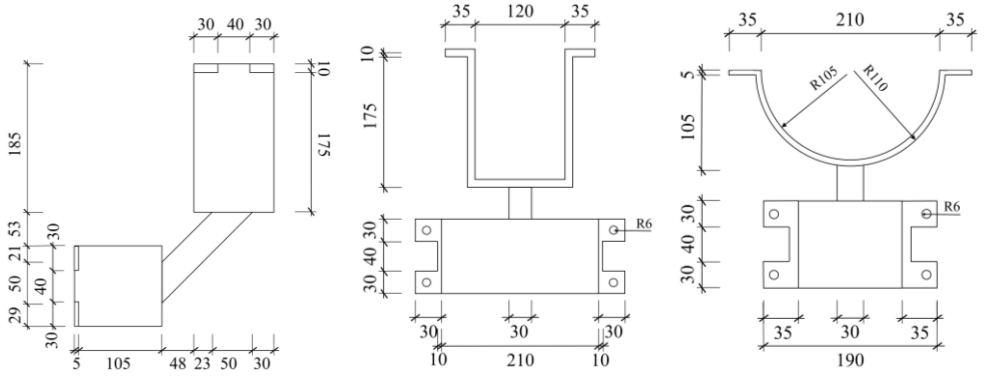

(a) Side view (b) Front view (c) Top view

Fig. 7 Detailed dimensions of beam-column support component

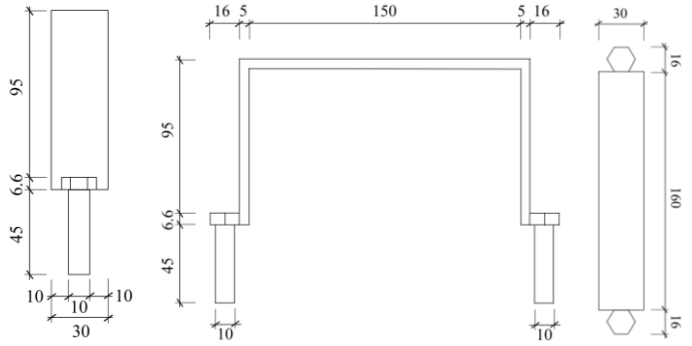

(a) Side view (b) Front view (c) Top view

Fig. 8 Detailed dimensions of column clamp hoops

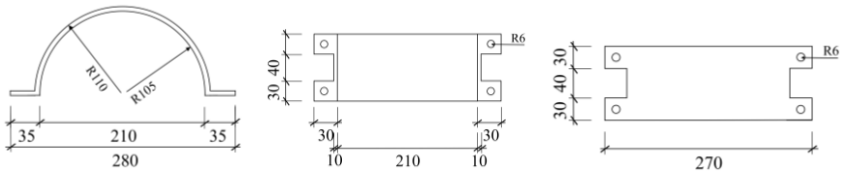

(a) Top view (b) Front view (c) Side view

Fig. 9 Detailed dimensions of Pu-pai Fang clamp hoops

Table 1
The degree of looseness of the dovetail mortise and tenon joint

Specimen	Dovetail mortise & tenon size(mm)			Reduction of tenon length (mm)	Degrees of loosening(%)
	c	a_1	a_2		
JR1	50	0	—	0	—
JR2	45	5	10%	5	10%
JR3	40	10	20%	10	20%
JR4	35	15	30%	15	30%

3.2. Test scheme

3.2.1. Loading equipment

The test loading device is shown in **Fig. 10**. The wooden column is placed horizontally on the base platform. Limit covers are installed respectively in the middle and at the end of the column to prevent the specimen from overturning and twisting during the loading process. The loading point is set at a distance of 500 mm from the upper edge of the column, and the low-cycle repeated load is jointly applied to the beam and the Pu-pai Fang by the test system (MTS actuator). To simulate the axial compression load formed by the transfer of the self-weight of the frame layer to the wooden columns, jacks are arranged in the horizontal direction of the columns, and a constant load of 20 kN is pre-applied to the column ends. A stable axial pressure is maintained throughout the entire cyclic loading process.

3.2.2. Measurement solution

The axial pressure of the column is measured by the load sensor integrated in the hydraulic jack. The displacement and load at the beam end are recorded by the load sensor within the MTS system. The load and displacement data were obtained by the DH3816 data acquisition instrument. The layout of the displacement meter is detailed in **Fig. 10**. The joint rotation θ is calculated by the difference between displacement meters W1 and W4, and the tenon pull-out and extrusion amounts are measured by W2 and W3.

3.2.3. Loading system

The quasi-static test loading system is designed in accordance with ISO 16670 [29] and adopts the loading mode of staged displacement control. The ultimate displacement of the joint is set at 50 mm, and the displacement amplitude is determined based on the ultimate displacement obtained from the monotonic loading test of the component. Single cycle loading was carried out respectively at 1.25 % (0.625 mm), 2.5 % (1.25 mm), 5 % (2.5 mm), and 10% (5 mm) of the set limit displacement. The three cycles of loading were carried out at 20 % (10 mm), 40 % (20 mm), 60 % (30 mm), 80 % (40 mm), 100 % (50 mm), and 120 % (60 mm) of the ultimate displacement respectively. The loading system is shown in **Fig. 11**.

If the following situations occur during the test: obvious plastic deformation or shear tearing occurs at the tenon or mortise; The rotation Angle significantly exceeds the limit value of 1/30 stipulated in the "Technical Standard for Maintenance and Reinforcement of timber Structures of Ancient Buildings" [30]. When the load drops to 80% of the peak load, the test should stop loading.

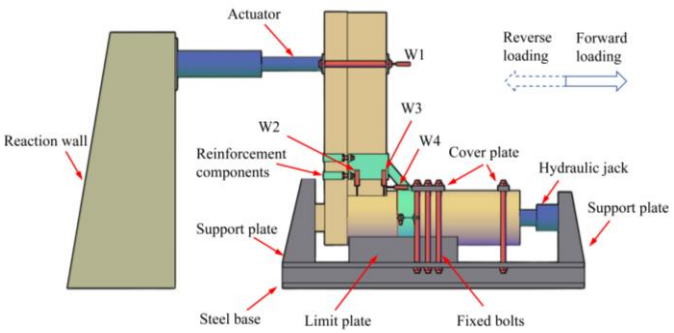

Fig. 10 Loading equipment

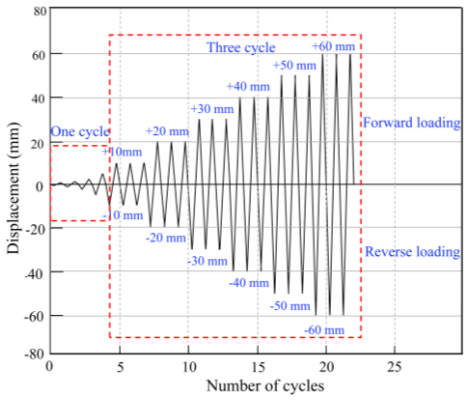

Fig. 11 Loading system

4. Test result and analysis

4.1. Test phenomenon

At the initial stage of loading, under the forward loading of JR1, the actuator drives the beam components to rotate, and the column and beam support components rotate synchronously, generating the sound of the column and beam support components being compacted. When reverse loading occurs, the tenon and the mortise generate extrusion friction along the contact surface, making a slight "creaking" sound of extrusion friction. The joint area remains in the elastic stage and no obvious plastic deformation has occurred.

When the rotation reaches 0.03rad, extrusion deformation occurs between the tenon and the mortise during forward loading, accompanied by the continuous sound of the column and beam supports being pushed and squeezed, as shown in **Fig. 12**(a). When loading in reverse, as the joints are constantly squeezed during the forward loading, only the squeezing and friction sounds of the wood being continuously pulled out can be heard during the reverse loading, while the clamps of the Pu-pai Fang are in an active state.

As the rotation continuously increases, the tenon constantly exhibits alternating pull-out and insertion behaviors during the loading process, and the wood fibers at the mortise are torn, as shown in **Fig. 12** (b). At this time, when loading in reverse, the clamping members of the Pu-pai Fang and the Pu-pai Fang continuously restrain the rotational deformation by adjusting the Angle, as shown in **Fig. 12** (c). But when a "bang bang" sound was heard from the wood, it was speculated that the fibers of the Pu-pai Fang had broken during its rotation.

When the joint rotation reaches 0.12rad, the tenon is continuously pulled out, with a tenon pulling amount of 18 mm, as shown in **Fig. 12** (d). At the mortise, the wood fibers are obviously lifted, resulting in significant deformation and damage. A continuous squeezing and stretching sound can be heard from the wood fibers of the Pu-pai Fang. During the loading process, the clamps of the Pu-pai Fang are in an active state, ensuring that the joints maintain the inherent seismic resistance and energy dissipation effect of the wood in the early stage of loading. In the later stage of loading, the clamps of the Pu-pai Fang can limit the free rotation of the joints through their own adjustment, significantly enhancing the tensile strength of the joints and reducing the pulling out of the tenons.

The test phenomena of JR2-JR4 are similar to those of the JR1 model, and the wood fibers at the joints all show severe warping. The difference lies in that no obvious sound of wood cracking occurred during the loading process. Meanwhile, for joints with different degrees of loosening, the pull-out amount in the later stage of loading was similar, but the pull-out rate of the tenon kept increasing as the degree of loosening increased.

(a) Initial loading stage (b) Onset of fiber tearing at the mortise (c) Progressive tenon pull-out under cyclic loading (d) Localized crushing & separation at joint interface

Fig. 12 Test phenomena of the Pu-pai Fang–dovetail tenon joint specimens

4.2. Analysis of seismic performance

4.2.1 Moment-rotation hysteretic curve

The Moment-Rotation hysteresis curves of specimens JR1-JR4 can be calculated respectively by Eqs. (1) and (2) :

$$M = FL \tag{1}$$

$$\theta = \frac{\Delta}{L} \tag{2}$$

where F is the horizontal load at the loading point of the MTS system, Δ is the horizontal displacement at the loading point, and L is the distance from the loading point to the surface of the column.

The moment-rotation hysteresis curves of JR1-JR4 are shown in **Fig. 13**(a), **Fig. 13**(b), **Fig. 13**(c) and **Fig. 13**(d), respectively. It is not difficult to find that the hysteresis curves of all joints all present an inverse Z-shaped feature and have obvious shrinkage characteristics, which is closely related to the material properties of timber structures. The hysteresis curve of the joint is relatively full at the initial stage of loading, and it has a good energy dissipation capacity. One reason is that during forward loading, the wood structure achieves structural energy dissipation through the compression and friction between components. On the other hand, during reverse loading, the beam-column support component has a large initial stiffness to limit the rotation of the joint. As the rotation of the joint increases, the interface sliding effect between the tenon and the mortise increases, and stiffness degradation and irreversible plastic deformation occur in the joint domain, with the hysteresis curve shrinking and narrowing. However, when the joint was loaded to the later stage, it did not enter the descent phase. This is because the Pu-pai Fang clamp hoops exerted a constraint on the reverse rotation of the joint, further increasing the overall load-bearing capacity of the structure.

By comparing the M_y and M_u of JR1-JR4 (**Table 2**), it is found that the yield bending moment and ultimate bending moment of JR2 are relatively large due to the overly tight installation process of the specimen. The remaining specimens show that the greater the degree of looseness of the joint, the greater the bending moment when entering the yield state. This is because the reduction of the tenon causes the Pu-pai Fang to need to provide greater structural resistance. The greater the degree of looseness of the joints, the greater the forward ultimate bending moment and the smaller the reverse ultimate bending moment. This is because when loading in the forward direction, the tenon pull-out rate increases, and the contact surface provided by the tenon to resist bending moment decreases, forcing the common beam to provide greater resistance to bending moment. However, when loading in the reverse direction, the tenon pull-out rate of JR1 is smaller, and the tenon can then provide greater resistance to bending moment.

Table 2
Comparison of characteristic values of the specimens

Specimen	Yield bending moment M_y (kN·m)	Ultimate bending moment M_u (kN·m)	Loading direction
JR1	1.09	12.42	Forward
	-4.58	-17.13	Reverse
JR2	4.01	16.51	Forward
	-6.58	-19.03	Reverse
JR3	3.00	13.06	Forward
	-4.23	-16.38	Reverse
JR4	2.72	14.99	Forward
	-6.54	-15.38	Reverse

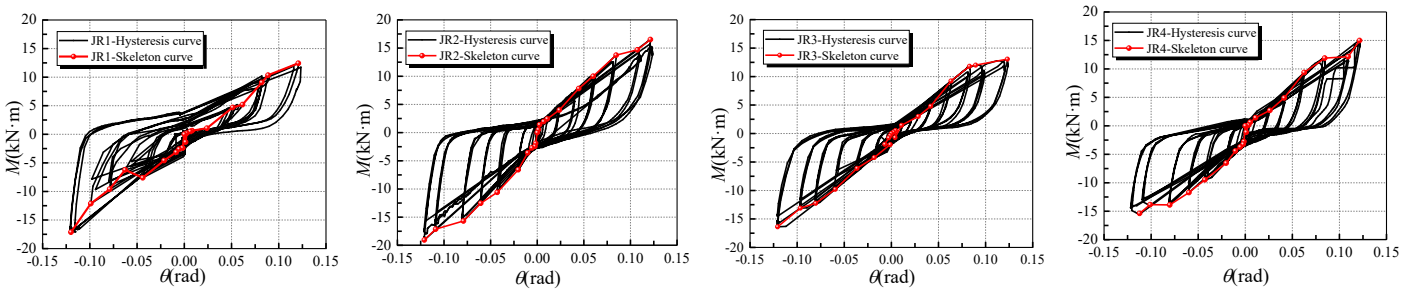

(a) JR1 (b) JR2 (c) JR3 (d) JR4

Fig. 13 Moment-rotation hysteresis curve of the joints

4.2.2. Moment-rotation skeleton curve

The envelope curves of the first maximum bending moment point in the moment-rotation curve under each stage displacement were taken as the skeleton curves, and a comparative analysis was conducted with the skeleton curves of the Pu-pai Fang - dovetail tenon joint in reference [13]. The comparison of the skeleton curves of JR1-JR4 and DJ1-DJ4 are shown in **Fig. 14**(a), **Fig. 14**(b), **Fig. 14**(c) and **Fig. 14**(d), respectively. The positive ultimate bending moment and negative ultimate bending moment of the intact joint JR1 have increased by 51.49% and 60.1% respectively. The positive ultimate bending moments and negative ultimate bending moments for the loose joints JR2-JR4 are respectively JR2: 96.58% and 89.39%. JR3: 50.89%, 164.58%; JR4: 92.16%, 58.96%. Compared with DJ1-DJ4, the bending moment values of JR1-JR4 in the early stage of loading are similar. However, in the later stage of loading, the overall flexural bearing capacity of the structure is significantly improved. The forward and reverse ultimate flexural bearing capacities of the reinforced specimens with different degrees of loosening exceed 50% compared with the unreinforced specimens. It indicates that the steel sleeve clamp hoops reinforcement can fully exert the energy dissipation and vibration reduction effect of the timber structure in the early stage of loading, and in the later stage of loading, the steel sleeve clamp further enhances the overall seismic performance of the structure.

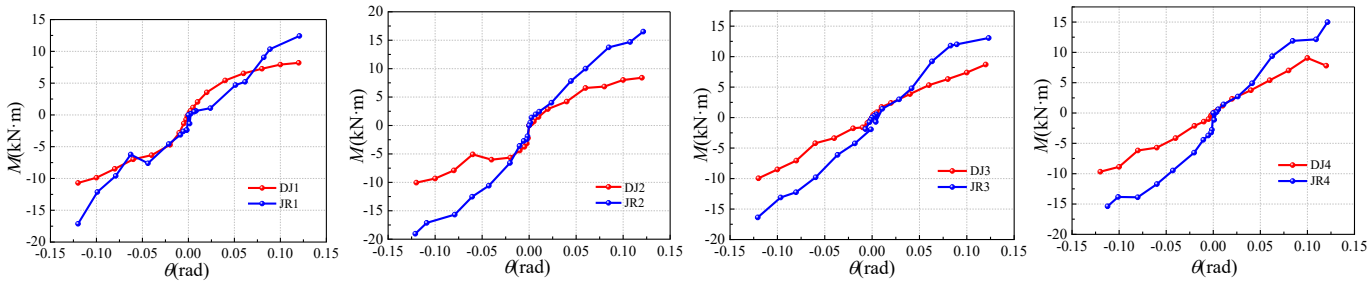

(a) DJ1 and JR1 (b) DJ2 and JR2 (c) DJ3 and JR3 (d)DJ4 and JR4

Fig. 14 Moment-rotation skeleton curve of specimens

4.2.3. Energy dissipation capacity

The equivalent viscous damping coefficient h_e directly reflects the energy dissipation capacity of the joint and can be calculated according to Eq. (3):

$$h_e = \frac{1}{2\pi}\frac{S_{(\Delta ABC+\Delta CDA)}}{S_{(\Delta EDO+\Delta FBO)}} \tag{3}$$

where $S_{(\Delta ABC+\Delta CDA)}$ represents the area enclosed by the shaded portion of the hysteresis loop **(Fig** 15), and $S_{(\Delta EDO+\Delta FBO)}$ denotes the triangular area corresponding to the hysteresis curve.

The equivalent viscous damping coefficient curves are shown in **Fig. 15**. The energy dissipation capacity of all specimens evolves similarly, initially rising rapidly to a peak value, followed by a gradual decline until reaching a stable state. However, when the rotation reaches 0.01 rad, h_e drops significantly. This is because energy dissipation occurs through compression and friction between components during rotation; as the gap between mortise and tenon gradually increases, the available free movement space expands, causing the joint to enter a loose state, thus leading to a progressive reduction in energy dissipation capacity. Subsequently, h_e continues to decrease and eventually stabilizes around 0.15. Comparing JR1–JR4 with DJ1–DJ4, it is observed that both types of joints exhibit similar trends in h_e, but the energy dissipation capacity of JR1–JR4 is superior to that of DJ1–DJ4, confirming the effectiveness of steel sleeve clamp hoops confinement in enhancing energy dissipation performance.

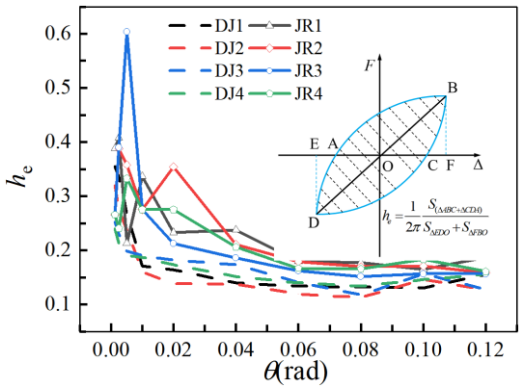

Fig. 15 Equivalent viscous damping coefficient of the joints

4.2.4. Stiffness degradation

The variation of secant stiffness at different deformation levels can reflect stiffness degradation. The secant stiffness K_i at each deformation level can be calculated according to Eq. (4):

$$K_i = \frac{|+M_i|+|-M_i|}{|+\theta_i|+|-\theta_i|} \tag{4}$$

where M_i is the peak bending moment of the first cycle under the i-th load level; θ_i is the rotation corresponding to M_i.

The stiffness degradation curve of the joint is shown in **Fig. 16**. During forward loading, the overall variation trends of JR1-JR4 are slightly different.

Generally, the initial stiffness of the joints rapidly deteriorates, then slowly increases and tends to a stable state to an average of 117.12 kN·m·rad^{-1}. JR1 has a relatively high resistance due to the resistance of the beam-column support components. Subsequently, during the rotation of the beam components, they are embedded with the beam-column support components, causing the material to soften and a large movable gap to appear at the contact interface. As a result, the stiffness rapidly decreases, among which the initial stiffness of JR1 deteriorates most obviously. The greater the degree of looseness of the joint, the larger the initial gap it already has, so the initial stiffness degradation is not obvious. This further indicates that steel sleeve clamp hoops are more suitable for reinforcing loose joints and can still maintain a certain initial stiffness at the joints.

When reverse loading is applied, the stiffness degradation trend of JR1-JR4 is generally consistent. The overall manifestation is that the initial stiffness of the nodes rapidly deteriorates, and then the stiffness degradation tends to stabilize to an average of 143.15 kN·m·rad^{-1}. This is because the Pu-pai Fang clamp hoops and beam-column supports form an active connection, and the initial loading does not interfere with the structure. To maximize the energy dissipation and shock absorption effect of the timber structure, the stiffness is kept stable in the later stage of loading by relying on the constraints of the Pu-pai Fang clamp hoops.

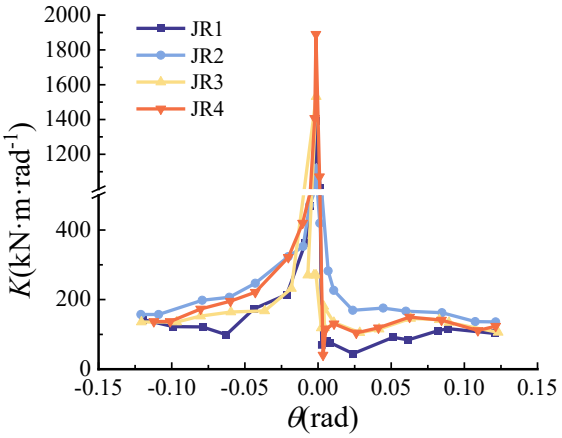

Fig. 16 Stiffness degradation curve of the joints

4.2.5. Deformation ability

The "GB 50165-2020 Technical Standard for Maintenance and Reinforcement of timber Structures in Ancient Buildings" clearly stipulates that the limit value of the displacement Angle at the beam-column joints of timber structures is 1/30. During the test loading process of JR1-JR4, the maximum rotation all reached 0.12 rad, and the joints maintained good bearing capacity. Their deformation capacity significantly exceeded the specification limit, fully verifying that this reinforcement method has excellent anti-deformation ability.

Fig. 17 shows the curve graph of the joint rotation and the tenon pull-out amount (γ). The average maximum tenon pull-out amount of JR1-JR4 is only 20.24 mm, and the tenon pull-out rates are 37.14 %, 50.74 %, 51.44 % and 54.25 % respectively. The tenon pull-out rate of JR1 is the lowest, indicating that the tenoning rate of the joint increases with the increase of the degree of loosening. By comparing the tenon pull-out rates of JR1-JR4 with those of DJ1-DJ4, it is not difficult to find that the overall tenon pull-out rate of JR1-JR4 is much lower than that of DJ1-DJ4, reducing by 53.51%, 13.41%, 46.89% and 46.25% respectively. Except for the fact that DJ2 is installed too tightly, The tenon extraction rates of the remaining joints can all be significantly reduced. During the reverse loading process of the joint, at the initial stage of loading, the joint is used for restraint, and energy is consumed through the compression and friction between the joint and the tenon. In the middle stage of loading, the Pu-pai Fang can provide resistance to bending moment for the rotation of the beam component. As the wood at the joint and the Pu-pai Fang is torn, the Pu-pai clamp hoop takes effect to achieve the function of constraining the rotation of the joint. At the same time, This also indicates that the steel sleeve clamp reinforcement has a significant effect on restricting the tenon pull-out.

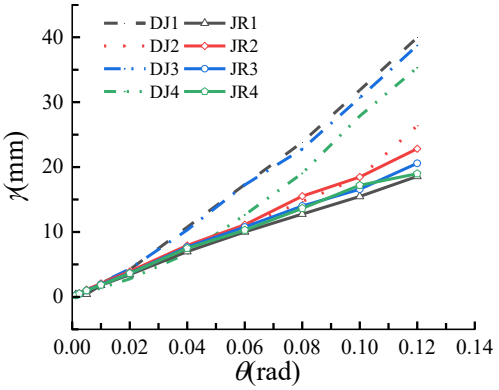

Fig. 17 Curves showing the relationship between joint rotation & tenon pull-out amount

5. Establishment of the finite element models

5.1. Model establishment

The finite element model (FEM) material was made of Masson pine. The material property parameters were obtained through tests. Its physical and mechanical properties were determined and completed by the members of the same research group [31] in accordance with the small sample testing methods stipulated in the Chinese National standard "Standard Test Methods for Physical and Mechanical Properties of Wood" [32-34]. The mechanical property parameters of this batch of Masson pine are shown in **Table 3**.

The model is established using the C3D8R type 8-node entity unit in ABAQUS, as shown in **Fig. 18**. As wood is an orthotropic material, the compression along the grain and transverse grain is simplified to a double-fold line model, and the tension is simplified to a single-fold line model. The elastic modulus of anisotropic materials in the elastic stage is defined using engineering constants. During the plastic stage, the yield stress of the material in different directions is determined by combining the potential function in ABAQUS with the Hill yield criterion. Steel and bolts are simulated as ideal elastoplastic materials. During the assembly process, assembly shall be carried out in accordance with the test design. A 2mm contact gap tolerance shall be reserved between the Pu-pai Fang and the Pu-pai Fang clamp hoops during the test process. The contact attributes between each component of the joint are defined through the interaction of surface-to-surface contact. Normal contact adopts "hard" contact to allow interface separation. The tangential behavior adopts a penalty function friction model. The friction coefficients between woods and between woods and steel are set at 0.3, and the friction between steel is set at 0.15. The model loading mode and boundary constraint conditions are consistent with the test conditions. The upper and lower ends of the column are respectively set as hinged and fixed connections, and the force application point is set at a position 500 mm away from the column surface. The boundary conditions are applied by coupling constraints through the initial analysis step. The test is divided into 4 analysis steps in total. It includes applying preload to the bolts, fixing the bolt length, applying axial load at the column end and low-cycle repeated load at the loading point, and setting the preload guarantee load F_p=25500N for the bolts [35].

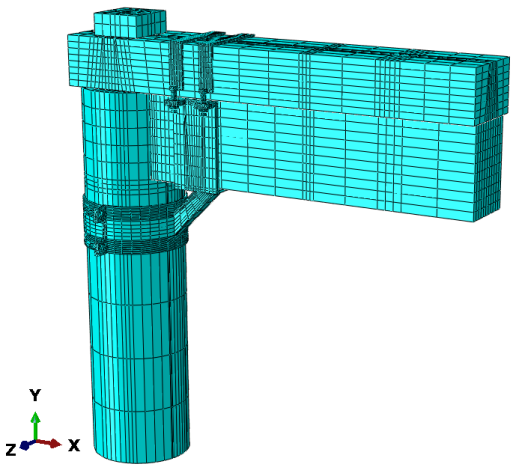

Fig. 18 Meshing details of finite element model

Table 3
Mechanical properties of *Pinus massoniana* Lamb

Parameter	Adopted value in FE model		
Density (kg/m3)	ρ=542		
Moisture content (%)	W=17		
Elasticity modulus (MPa)	E_L=19411	E_R=1465	E_T=762
Poisson ratio	μ_{LR}=0.28	μ_{LT}=0.48	μ_{RT}=0.62
Shear modulus (MPa)	G_{LR}=1456	G_{LT}=1165	G_{RT}=349
Yield stress (MPa)	f_{tL}=120.9	f_{cL}=31.08	f_{cR}=3.62
Yield stress ratio	R_{11}=1	R_{22}=0.12	R_{33}=0.12
	R_{12}=0.56	R_{13}=0.56	R_{23}=0.13

Note: ρ and W denote the density and moisture content; L, R, and T denote the longitudinal, radial, and tangential directions of wood grain, respectively; μ is the Poisson ratio; E is the elastic modulus; G is the shear modulus; f_{tL} is the tensile strength parallel to the grain; f_{cL} is the compressive strength parallel to the grain; f_{cR} is the compressive strength perpendicular to the grain.

5.2. Model verification

The stress distributions of the finite element model failure modes under forward loading and reverse loading are shown in Fig. 19(a) and Fig. 19(b) respectively. The finite element model and the test results were compared. The hysteresis curves of JR1-JR4 are shown in **Fig. 20**(a), **Fig. 20**(b), **Fig. 20**(c), and **Fig. 20**(d). Except for JR2 which was too tight during the test installation process, the comparison results at M_E and M_T of the other specimens are in good agreement (**Table 4**), and the error ratio between the test results and the finite element prediction results is all less than 20%. It indicates that the finite element results are in good consistency with the experiments. The hysteretic curves of the test specimens are fuller than those of the finite element model. This is because during the test, the wood fibers at the common beam and the joint of the specimen successively cracked and broke, the movable gap of the tenon increased, and the sliding effect of the contact interface at the joint increased during the reciprocating loading process.

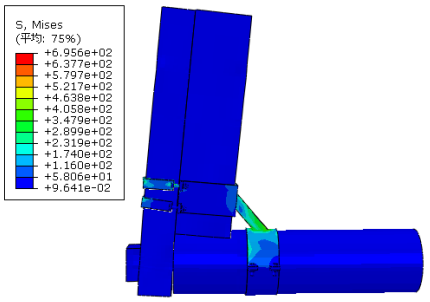

(a) Forward loading

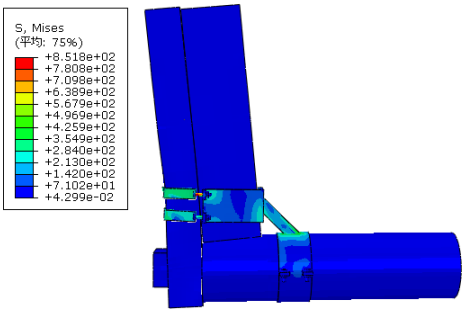

(b) Reverse loading

Fig. 19 Stress contour with the failure modes

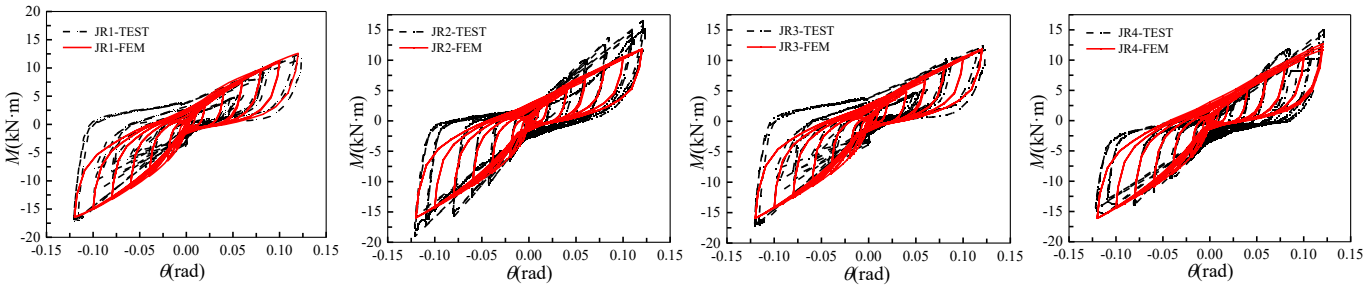

(a) JR-1 (b) JR-2 (c) JR-3 (d) JR-4

Fig. 20 Comparison between the finite element model and test results

Table 4
Comparison between experimental and FE results

Specimen	M_E (kN·m)	M_T (kN·m)	Error rate (%)
JR1	-16.43	-17.13	4.22
	12.59	12.42	1.35
JR2	-15.93	-19.03	16.31
	11.82	16.51	28.41
JR3	-15.93	-16.38	2.73
	11.82	9.47	9.47
JR4	-16.14	-15.38	4.72
	12.65	14.99	15.63

5.3. Parameters influence analysis

5.3.1. Friction coefficient

The friction coefficients of u=0.1, 0.3, 0.5 and 0.7 were selected for analysis respectively, as shown in **Fig. 21**. When subjected to reverse loading, the flexural bearing capacity of the joint increased from 14.91 kN·m to 18.94 kN·m, an increase of 27.04%. This indicates that the flexural bearing capacity of the joint increases with the increase of the friction coefficient. During forward loading, the high friction characteristic can provide stiffness at the initial stage of loading, but it may cause brittle failure of the structure in the later stage of loading, reducing the seismic toughness. Meanwhile, the high friction characteristic is contrary to the principle of using Pu-pai Fang clamp hoops for movable reinforcement. However, when the friction coefficient is within the range of 0.3 to 0.5, the structure strikes a balance between strength and ductility, improving rotational stiffness. Enhancing the moment bearing capacity can effectively achieve energy dissipation. Therefore, it is recommended that the friction coefficient be selected as 0.3 to 0.5, which is more appropriate.

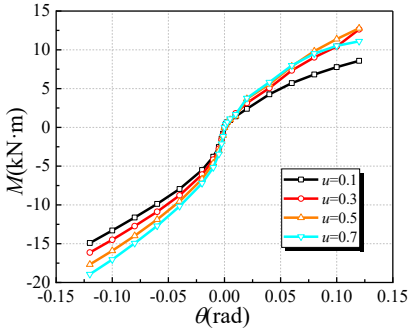

Fig. 21 Friction coefficients of joints

5.3.2. Bolt preload

The preload forces of the welding bolts were selected as f_1=0.25 F_p, f_2=0.5 F_p, f_3=0.75 F_p and f_4= F_p respectively, as shown in **Fig. 22**. It can be seen that the preload force of the welding bolts has little effect on the bearing capacity under reverse loading, while under forward loading, the flexural bearing capacity increases with the increase of the preload force. The increase was from 12.27 kN·m to 12.65 kN·m, representing only a 3.07 % increase. This indicates that applying preload to bolts is an important step in the reinforcement of steel sleeve clamp hoops. However, the magnitude of the preload has a relatively small impact on the flexural bearing capacity of the structure. This also suggests that the key point of this reinforcement device lies in reducing intervention in the early stage of loading This purpose of providing protective effects on the structure in the later stage of loading is consistent.

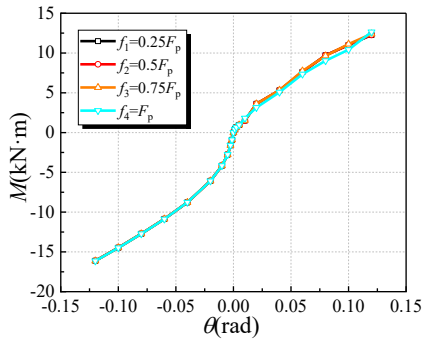

Fig. 22 Bolt preload of the joints

5.3.3. Pu-pai Fang Clamp hoop thickness

The thicknesses h of the Pu-pai Fang clamp hoops was selected as 3 mm, 5 mm, 7 mm and 9 mm, as shown in **Fig. 23**. When reverse loading was applied, the flexural bearing capacities of the models with h=3 mm, h=5 mm, and h=7 mm were similar. However, when the thickness increased to 9 mm, the flexural bearing capacity of the models decreased from 16.14 kN m to 13.32 kN m, a reduction of 17.4 %. When subjected to forward loading, the flexural bearing capacities of the models h=5 mm and h=7mm are 12.40 kN·m and 12.28 kN·m respectively. These flexural bearing capacities are significantly better than those of the models h=3mm and h=9mm, indicating that a thickness range of 5-7mm is more suitable for the clamp hoop parts of the Pu-pai Fang.

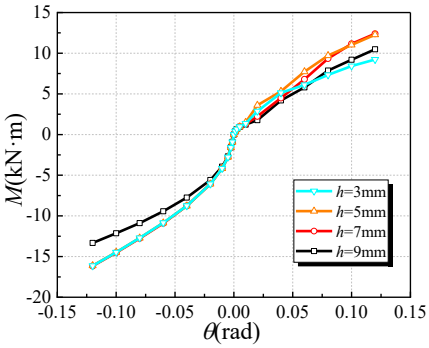

Fig. 23 Pu-pai Fang clamp hoop thickness of joints

6. Conclusions

This study investigated the seismic performance of Pu-pai Fang–dovetail tenon joints with different degrees of looseness reinforced by steel sleeve clamp hoops through quasi-static testing and finite element (FE) simulation. The main conclusions are summarized as follows:

(1) Due to the continuous alternating pull-out and insertion of the intact specimens, the wood fibers at the mortise and the Pu-pai Fang were torn. In the later stage of loading, the Angle of the Pu-pai Fang clamp hoops was adjusted to restrict the free rotation of the joints, enhancing the tensile pull-out capacity of the joints and reducing the pull-out of the tenons. The damage phenomenon of the loose joints was similar to that of the intact specimens, and the pull-out amount of the tenons was also similar. However, the tenon pull-out rate keeps increasing as the degree of loosening increases.

(2) The hysteresis curve of the joint shows an inverse Z-shaped feature. There is a significant shrinkage characteristic in the later stage of loading. However, the steel sleeve clamp hoop exerts a constraint on the reverse rotation of the joint, further increasing the flexural bearing capacity, and no decline stage occurs. The greater the degree of joint loosening, the greater the forward ultimate bending moment and the smaller the reverse ultimate bending moment. The forward and reverse ultimate flexural bearing capacities of the reinforced specimens exceed 50% compared with those of the unreinforced specimens.

(3) The energy consumption capacity characteristic of the joint is characterized by a rapid increase to the peak in the initial stage, followed by a slow decline and a gradual stabilization. The stiffness degradation characteristics of the joint are manifested as a rapid initial stiffness degradation, followed by a slow increase and a tendency towards a stable state. The average maximum tenon extraction amount of the joints was only 20.24 mm, and the tenon extraction rates were 37.14 %, 50.74 %, 51.44 % and 54.25 % respectively. Compared with the unreinforced joints, the tenon extraction rates decreased by 53.51 %, 13.41 %, 46.89 % and 46.25 % respectively. The main reason lies in the fact that the steel sleeve clamp reinforcement maintains the energy dissipation of the wooden structure in the early stage of loading and constrains the energy dissipation in the later stage of loading.(4) It is recommended that the coefficient of friction be set within the range of 0.3 to 0.5, and the thickness of the Pu-pai Fang clamp hoop be set within the range of 5 to 7mm. This can balance the structural strength and ductility, improve the rotational stiffness, enhance the moment bearing capacity, and effectively achieve energy dissipation. Applying preload to bolts has no obvious effect on the reinforcement of steel sleeve clamp hoops.

Acknowledgements

The work was financially supported by the grant from the Basic and Applied Basic Research Foundation of Guangdong Province (Grant No. 2025A1515010443) and the Scientific and Technological Achievements Transformation Project of the Scientific Research Institutes of Science and Technology Department of Sichuan Province (Grant No. 2024ZHYS0008).

References

[1] Pan Y., An R.B. and You. W.L., “A review on mechanical performance of mortise-tenon joints in traditional timber structures”, *Journal of Building Structures*, 45(07): 226-241, 2024.
[2] Wu Y.J., Wang L., Lin H.S., Zhang L.P. and Xie. Q.F., “Effect of shear force on the rotational performance of straight mortise-tenon joints”, Structures, 44: 501-10, 2020.
[3] Wang J., Cui Z.H., Yu L., Xu R.W. and Yang. Q.S., “Analysis of the seismic behavior of traditional Chinese timber structures in the tang dynasty”, Structures, 41: 447-62, 2022.
[4] Wang S.Y., Guo T., Deng H. and Zhou. H.B., “Study on seismic performance of straight Tenon-type joints in Chuan-dou style timber structure”, Chinese Journal of Wood Science and Technology, 36(01): 57-62, 2022.
[5] Wang Q.L. Ye J.H. and Su M.Z., “Cyclic behavior and shear capacity of a single-frame modular steel structure-cold-formed steel wall with semi rigid connections”, Advanced Steel Construction, 21(4):304-315, 2025.
[6] Bai F.Y., Fan Z.K., Xue J.Y., Wu C.W., Hu C.M. and Li. J.X., “Experimental study on seismic performance and deformation damage of loose dovetail-tenon joints in ancient timber structures”, Structures, 54, 541-555, 2023.
[7] Zhang J, Li Y.H., LI Y.J., Xu W.T. and Yao. L.H., “Research on Stress Analysis of Dovetail Joints of Timber Building”, China Forest Products Industry, 58(03): 21-26, 2021.
[8] Yu P., Li T.Y., Yang Q.S. Meng X.J., Shi X.W. and Chen. J.Y. “Analytical model and rotational performances of dovetail mortise-tenon connection at the column head of traditional wooden frame”, Structures, 57,105256, 2023.
[9] Zhang B.Z., Xie Q.F., Li S.Y., Zhang L.P. and Wu. Y.J., “Effects of gaps on the rotational performance of traditional straight mortise-tenon joints”. Engineering Structures, 260: 114231, 2022.
[10] Bai F.Y., Fan Z.K., Xue J.Y., Wu C.W., Hu C.M. and Li. J.X., “Experimental study on seismic performance and deformation damage of loose dovetail-tenon joints in ancient timber structures”. Structures, 54: 541–55, 2023.
[11] Bai F.Y., Dong F., Sui Y., Xue J.Y., Wu C.W., Song D.J. and Hu. C.M., “Experimental study on fracture damage and seismic performance of loose through-tenon joints in ancient timber structures”. Construction and Building Materials, 394: 132228, 2023.
[12] He J.X., Yu P., Wang J., Yang Q.S., Han M. and Xie. L.L., “Theoretical model of bending moment for the penetrated mortise-tenon joint involving gaps in traditional timber structure”. Journal of Building Engineering, 42, 103102, 2021.
[13] Chu Y.P., Tan S.L., Gu S. and Wang. S.Q., “Seismic performance of Pu-Pai Fang- Dovetail mortise and tenon joints at different degrees of looseness: experimental tests and theoretical analysis”, International journal of architectural heritage, 1–24, 2025.
[14] Wu Y.J., Lin H.S., Xie Q.F. Wang L. and Zhang. L.P., “Influence of Pu-pai Fang on lateral performance of columns in ancient timber structures”, Journal of Building Structures, 44(11): 170-180, 2023.
[15] Chu Y.P., Li Q., Zeng M.Q., Wang J.H. and Gu. S., “Seismic performance of cross hoop-head mortise and tenon joints under different degrees of looseness”, Structures, 81, 110268, 2025.
[16] Dong H.Y., Jin Y.J., Cao W.L., Liang X, Liu. S.Y., “Seismic performance of wooden straight-tenon joints reinforced with lightweight steel members”, Engineering Structures, 282, 115825, 2023.
[17] Xue J.Y., Wu C.W., Zhang X.C. and Zhang. Y.T., “Experimental study on seismic behavior of mortise- tenon joints reinforced with shape memory alloy”. Engineering Structures 218: 110839, 2020.
[18] Xue J.Y., Wu C.W., Zhang X.C. and Qi. Z.D., “Experimental and numerical study of mortise-tenon joints reinforced with innovative friction damper”. Engineering Structures, 230: 111701, 2021.
[19] Chen J., Wang W., Ding F.X., Xiang P., Yu Y.J., Liu X.M. Xu F. Yang C.Q. and Long. S.G., “Behavior of an advanced bolted shear connector in prefabricated steel-concrete composite beams”, Materials, 12(18): 2958, 2019.

[20] Xie Q.F., Zhang L.P., Zhou W.J., Wang L. and Zhou. T.G., "Cyclical behavior of timber mortise-tenon joints strengthened with shape memory alloy: experiments and moment-rotation model". International journal of architectural heritage, 13(8): 1209-22, 2018.
[21] Latour M., Piluso V. and Rizzano. G., "Experimental analysis of beam-to-column joints equipped with sprayed aluminium friction dampers". Journal of Constructional Steel Research, 146: 33-48, 2018.
[22] Tan J.P., Pan D.G. and Fu X.Q., "Seismic Performance Evaluation of Steel Frames with Dampers AddED on Existing Structures", Advanced Steel Construction, 18 (2) 552-560, 2022.
[23] He J.X., Liu K., Xie L.L., Wang. X.J., Yang W.Y. and Zhao W.L., Experimental and numerical studies on influences of wedge reinforcement on seismic performance of loose penetrated mortise-tenon joints, Journal of Building Engineering, 91, 109610, 2024.
[24] Li Jie. Yingzao fashi (tandards and Models for Architecture). Royal. Kaifeng: Press; 1950.
[25] Yu P., Yang Q.S., Li T.Y., Meng X.J., Shi X.W. and Chen. J.Y., "Quantitative contribution assessment of joints and components to the load-carrying capacity of ancient timber frame", Structures, 59, 105739, 2024.
[26] Qin Z.C., Moriyama H., Yamaguchi T., Shigeishi M., Xing Y.Y. and Hashimoto. A., "Ultimate strength, ductility, and failure mode of high-strength frictional frictional bolted joints made of", Advanced Steel Construction. 19, 117–22, 2023.
[27] Gan D., Tang H.X., Li W., Zhou Z., Zhou X.H. and Chen. Z.M., "Analysis and design of axialysis and design of axially loaded square CFST column to RC beam joints stiffened by diagonal ribs", Advanced Steel Construction, 19(1):38-45, 2023.
[28] Jakovljević I., Spremić M. and Marković. Z., "Shear behaviour of demountable connections with bolts and headed studs", Advanced Steel Construction, 19(4): 341-352, 2023.
[29] ISO-16670. Timber structure-Joints made with mechanical fasters-Quasi-static. reversed cyclic test method. International Organization for Standard; 2003.
[30] GB 50165-2020. Technical standard for maintenance and reinforcement of ancient timber structures, Beijing, China, 2020.
[31] Chu Y.P., Shi B.X. and Gong. Y.D., "Experimental study on compressive behavior of intermediate slender timber columns with local damage and the retrofitting techniques for the damaged columns", Structures, 46, 1709-1725, 2022.
[32] GB/T 1927.1-2021. Test methods for physical and mechanical properties of small clear wood specimens-Part 9: determination of bending strength, Beijing, China, 2021.
[33] GB/T 1927.1-2021. Test methods for physical and mechanical properties of small clear wood specimens-Part 10: determination of bending modulus of elasticity, Beijing, China; 2021.
[34] GB/T 1927.1-2021. Test methods for physical and mechanical properties of small clear wood specimens-Part 12: determination of radial compressive strength. Beijing, China; 2021.
[35] GB/T 3098.1-2010. Mechanical properties of fasteners-Bolts, screws and studs. Beijing, China, 2010.